DOI: 10.1534/genetics.107.084905

Genetic Modification of the Schisis Phenotype in a Mouse Model of X-Linked Retinoschisis

Britt A. Johnson, Natsuyo Aoyama, Nicole H. Friedell, Sakae Ikeda and Akihiro Ikeda[1]

Department of Medical Genetics, University of Wisconsin, Madison, Wisconsin 53706

Manuscript received November 23, 2007
Accepted for publication January 14, 2008

ABSTRACT

X-linked retinoschisis (XLRS) is an inherited form of macular degeneration that is caused by mutations in the retinoschisin (*RS1*) gene. In addition to macular degeneration, other major characteristics of XLRS include splitting of the retina (schisis) and impaired synaptic transmission as indicated by a reduction in the electroretinogram b-wave. It has been known that patients carrying *RS1* mutations show a broad range of phenotypic variability. Interestingly, phenotypic variation is observed even among family members with the same *RS1* mutation, suggesting the existence of genetic or environmental factors that contribute to the severity of XLRS. However, in the human population, the cause of phenotypic variability and the contribution of genetic modifiers for this relatively rare disease are difficult to study and poorly understood. In this study, using a mouse model for XLRS, we show that genetic factors can contribute to the severity of the retinoschisis phenotype. We report evidence of a major genetic modifier of *Rs1*, which affects the disease severity in these animals. A quantitative trait locus (QTL), named **m**odifier **o**f ***Rs1*** **1** (*Mor1*), is mapped on chromosome (Chr) 7. When homozygous, the *Mor1* allele from the inbred mouse strain AKR/J diminishes the severity of the schisis phenotype in $Rs1^{tmgc1}$/Y male and $Rs1^{tmgc1}/Rs1^{tmgc1}$ female mice. We also show that the penetrance of the disease phenotype is affected by additional genetic factor(s). Our study suggests that multiple genetic modifiers could potentially be responsible for the phenotypic variation in human XLRS.

X-LINKED retinoschisis [XLRS; Online Mendelian Inheritance in Man (OMIM) 312700] is a juvenile form of macular degeneration that affects male children with an incidence of 1 in 5000 to 1 in 25,000 (George *et al.* 1995b). XLRS is characterized by foveal schisis (splitting of the central retina), degeneration of the vitreous and retina, and reduced synaptic transmission characterized by a reduction in the electroretinogram (ERG) b-wave (Peachey *et al.* 1987; George *et al.* 1996; Retinoschisis Consortium 1998; Seiving 1998). Roughly 50% of XLRS patients have peripheral retinoschisis (Roesch *et al.* 1998; Pimenides *et al.* 2005).

XLRS is caused by mutations in the *RS1* gene (formerly *RS*; Sauer *et al.* 1997). Over 150 allelic variants of *RS1* mutations have been identified to date (X-Linked Retinoschisis Sequence Variation database at http://www.dmd.nl/rs/). XLRS patients exhibit a broad range of phenotypic severity. For example, the maculopathy observed in patients ranges from foveal radial striations and microcystic macular lesions to large atrophic macular lesions (Harris and Yeung 1976; Roesch *et al.* 1998). Other complications observed in some patients include retinal detachment, vitreous hemorrhage, nystagmus, and neovascular glaucoma (Kellner *et al.* 1990; Pimenides *et al.* 2005). Specific mutations have not been found to correlate with phenotypic severity (Shinoda *et al.* 1999; Eksandh *et al.* 2000; Hiraoka *et al.* 2000; Nakamura *et al.* 2001; Simonelli *et al.* 2003; Hewitt *et al.* 2005; Pimenides *et al.* 2005). Even family members with the same mutation exhibit large variation in phenotypic severity (Eksandh *et al.* 2000; Pimenides *et al.* 2005). This large intrafamilial and interfamilial phenotypic variation suggests the existence of genetic modifiers or differential susceptibility to environmental factors.

Human *RS1* is composed of 6 exons encoding the 224-amino acid protein, retinoschisin (RS1) (Sauer *et al.* 1997). The expression of RS1 has been detected in the retina (Sauer *et al.* 1997) and the pineal gland (Takada *et al.* 2006). In the retina, RS1 is synthesized in the photoreceptor cells (Reid *et al.* 1999) and other retinal neurons (Molday *et al.* 2001; Weber *et al.* 2002; Takada *et al.* 2004). The 24-kDa protein contains an N-terminal leader sequence which is cleaved for secretion, an RS1 domain that is important for higher order structure (Wu and Molday 2003), and a highly conserved discoidin domain. The discoidin domain is the major feature of RS1, comprising >75% of the processed protein (Sauer *et al.* 1997). Discoidin domains are found in a wide range of proteins involved in cell adhesion and cell–cell interactions, implicating RS1 in retinal cell adhesion (Baumgartner *et al.* 1998). Once processed, RS1 assembles into a disulfide-linked homooctamer (Wu *et al.* 2005). Recently, it was shown that RS1 interacts with a Na/K ATPase-SARM1 complex to anchor

[1]*Corresponding author:* Department of Medical Genetics, Room 5350 Genetics/Biotech, 425-G Henry Mall, University of Wisconsin, Madison, WI 53706. E-mail: aikeda@wisc.edu

to the photoreceptor and bipolar cell membrane (Molday *et al.* 2007). However, the manner by which RS1 mediates cell adhesion remains to be determined.

Two gene-targeted mutants (Weber *et al.* 2002; Zeng *et al.* 2004) and one ENU-induced splice-site mutant (Jablonski *et al.* 2005a) have been generated in the murine *RS1* homolog, *Rs1*. These mutant mice have phenotypes similar to human XLRS patients such as b-wave loss, photoreceptor cell degeneration, and schisis (Weber *et al.* 2002; Zeng *et al.* 2004; Johnson *et al.* 2006), showing that the mouse can serve as a model to study XLRS. Research on XLRS mouse models has also identified phenotypes that cannot be easily studied in human patients. Previously, we showed that the splice-site mutant, 44TNJ ($Rs1^{tmgc1}/Rs1^{tmgc1}$ and $Rs1^{tmgc1}$/Y), has reduced synaptic vesicle density in the photoreceptor cells and ectopic synaptic localization in the outer retina (Johnson *et al.* 2006). In studies using $Rs1^{-}$/Y gene targeted mice, gene therapy has been shown to restore the b-wave loss (Zeng *et al.* 2004; Min *et al.* 2005). Further studies in these mouse models may provide key insights into the pathological mechanisms and treatment of human XLRS.

Modifier screening allows for the identification of loci that interact with a primary Mendelian trait or disease of interest (reviewed in Nadeau 2001, 2003). The heterogeneous nature of human populations and the variability of possible environmental influences make modifier screening in humans difficult. To overcome this challenge, modifier screens in mouse models can be used to identify modifiers in genetically homogeneous populations and controlled environments. A genetic modifier that is identified in the mouse can then be tested for its affect on disease in humans. As an example, a modifier of obesity-induced type 2 diabetes, *Sorcs1*, originally identified in the mouse (Clee *et al.* 2006) was recently linked to diabetes susceptibility in humans (Goodarzi *et al.* 2007). A modifier of mammary tumor susceptibility, deleted in malignant brain tumors 1 (*Dmbt1*), was also originally identified in the mouse and then linked to mammary tumor susceptibility in humans (Blackburn *et al.* 2007). These examples illustrate that modifier screening in the mouse provides a powerful tool to identify modifiers of human disease.

In this study, we report the identification of a major quantitative trait locus (QTL), named **m**odifier **of *Rs1* 1** (*Mor1*). The AKR protective allele of the *Mor1* locus restores cell adhesion in $Rs1^{tmgc1}/Rs1^{tmgc1}$ and $Rs1^{tmgc1}$/Y mutant mice when homozygous. This report marks the first evidence that genetic modifiers influence the disease severity in *Rs1* mutant mice and suggests similar genetic factors may influence XLRS disease severity.

MATERIALS AND METHODS

Congenic mice and crosses: All mouse procedures were performed in accordance with the Association for Research in Vision and Ophthalmology's statement for the use of animals in ophthalmic and vision research. 44TNJ ($Rs1^{tmgc1}/Rs1^{tmgc1}$ and $Rs1^{tmgc1}$/Y; formerly $Rs1h^{tmgc1}$) mice were obtained from the Tennessee Mouse Genome Consortium (TMGC) ENU mutagenesis project. These mice are on a genetic background that is a mixture of C57BL/6J (B6) and C3Sn.BliA-*Pde6b*$^{+}$ (C3H) (Jablonski *et al.* 2005a,b). No gender-specific differences in the retinal phenotype were found among affected mice. Age-matched wild-type AKR/J (AKR), B6, and C3H mice were obtained from The Jackson Laboratory (Bar Harbor, ME). To generate the F_2 intercross, F_1 progeny from breeding pairs of AKR females and $Rs1^{tmgc1}$/Y males were intercrossed to produce 270 (AKRx$Rs1^{tmgc1}$/Y) $Rs1^{tmgc1}$/Y F_2 males. To generate the B6 congenic strain, F_2 $Rs1^{tmgc1}$/+ females containing a donor AKR segment from marker D7Mit310 to D7Mit237 were sequentially backcrossed to B6 for five to nine generations and intercrossed to yield mutant mice that were AKR, B6, or heterozygous for the chromosome (Chr) 7 introgressed region. No genotyping was performed for analysis of markers flanking either the introgressed region or elsewhere in the genome. To generate the C3H congenic strain, $Rs1^{tmgc1}/Rs1^{tmgc1}$ females were sequentially backcrossed to C3H for five to nine generations. Except for the *Rs1* locus, these mice are homozygous for C3H across the entire genome.

Histology: Following asphyxiation by CO_2 administration, eyes were immediately removed and immersion fixed in Bouin's fixative overnight at 4°. Eyes were then rinsed, dehydrated, and embedded in paraffin. Paraffin blocks were sectioned 6-μm thick on an RM 2135 microtome (Leica Microsystems, Wetzlar, Germany) and mounted on glass slides. Following hematoxylin and eosin (H&E) staining, slides were imaged on an Eclipse E600 microscope (Nikon, Tokyo) using a SPOT camera (Spot Diagnostics, Sterling Heights, MI).

Electroretinograms: Electroretinograms were recorded from 4-week-old $Rs1^{tmgc1}/Rs1^{tmgc1}$ and $Rs1^{tmgc1}$/Y ($n = 5$), 9-week-old $Rs1^{tmgc1}/Rs1^{tmgc1}$ and $Rs1^{tmgc1}$/Y ($n = 6$), and 4- and 9-week-old B6 wild-type ($n = 6$, $n = 5$, respectively) mice as previously described (Pinto *et al.* 2004). Briefly, mice were dark-adapted for at least 2 hr prior to recording and all procedures were performed in total darkness. After being anesthetized with ketamine (70 mg/kg) and xylazine (7 mg/kg), mice were placed in the recording chamber on a heating pad to maintain body temperature at 37°. Mice were fitted with DTL fiber electrodes on each eye and the electroretinogram recorded differentially between the eyes. After the corneas were moistened with 0.9% NaCl, one eye was covered with a clear contact lens and the other with an opaque contact lens. Nine full-field flash stimuli [luminance 7×10^{-4} to 300 candela (cd) sec/m^2] were presented to the eye covered with the clear lens against a dark background and a dim adapting light (0.5 cd/m^2) was presented steadily to light-adapt the retina while a flash stimulus (luminance 0.2 cd sec/m^2) was presented to evoke the cone electroretinogram. Electroretinograms were differentially amplified (0.1–1000 Hz) and recorded at 1 kHz with a resolution of 0.5 μV. The amplitude of the a-wave was measured from the prestimulus baseline to the peak of the a-wave. The amplitude of the b-wave was measured from the peak of the a-wave to the peak of the b-wave, or from the prestimulus baseline if no a-wave was present. All data in the luminance series were analyzed by a two-way analysis of variance (ANOVA) using GraphPad Prism software (GraphPad, San Diego). The b/a-wave ratios were analyzed by one-way ANOVA.

QTL and statistical analysis: We performed an initial whole genomewide scan using 45 $Rs1^{tmgc1}$/Y F_2 intercross mice. We selected 80 microsatellite markers that distinguish both B6 and C3H alleles from AKR alleles across the whole genome. All F_2 animals were phenotyped by histological analysis irrespective of genotyping. Affected animals were independently

scored by four people in a semiquantitative fashion. The four observers' scores were averaged to reduce human error. Scores ranged from zero to two (from wild type to severe, respectively) for schisis (Figure 2). QTL analysis was performed using the R/qtl statistical package (http://www.rqtl.org/) (Broman *et al.* 2003). To calculate LOD scores, R/qtl first generated a genetic map on the basis of the data of our cross. LOD scores were calculated using the multiple-imputation method (Sen and Churchill 2001) with 1-cM steps, 1000 joint genotype distribution imputations, and an assumed genotyping error rate of 0.01. To determine the significance of the results, a permutation test with 1000 replications was used. After the initial linkage on Chr 7 was determined, 225 additional $Rs1^{tmgc1}$/Y F_2 mice were phenotyped and genotyped for Chr 7 markers. QTL analysis was then performed on all 270 mice. For comparing the phenotypic distribution of the different F_2 genotypes (Figure 3) and the B6 congenic genotypes (Figure 4), one-way ANOVA with Bonferroni correction was calculated using GraphPad Prism software (GraphPad). To compare the penetrance of the schisis phenotype between the B6 and C3H congenic lines (Figure 5), GraphPad Prism software (GraphPad) was used to generate a 2 × 2 contingency table and calculate the resulting χ^2-value.

Quantifying the ratio of differentially spliced transcripts from *Rs1*: Total RNA was extracted with Trizol (Invitrogen, Carlsbad, CA) from one retina of 4-week-old $Rs1^{tmgc1}/Rs1^{tmgc1}$ and $Rs1^{tmgc1}$/Y ($n = 4$), 16-week-old $Rs1^{tmgc1}/Rs1^{tmgc1}$ ($n = 3$), 4-week-old $Mor1^{AKR}/Mor1^{AKR}$ ($n = 4$), and 4-week-old $Mor1^{B6}/Mor1^{B6}$ ($n = 3$) mice. Three hundred fifty nanograms of total RNA from each sample were converted to cDNA using the Superscript III first-strand synthesis system (Invitrogen) according to the manufacturer's instructions. Each sample was amplified in triplicate for the *Rs1* gene. A detailed protocol for RT–PCR and primer sequences were previously described (Johnson *et al.* 2006). After amplification, RT–PCR products were dried in a speed-vac concentrator and resuspended in 2 μl of water. One microliter of product was separated for fragment analysis on an Agilent 2100 bioanalyzer with a DNA 7500 kit according to the manufacturer's instructions (Agilent Technologies, Palo Alto, CA). Fragment analysis was conducted using samples collected after every 2 cycles between 20 to 30 cycles. The data presented here are for samples where amplification was in the linear range. Time-corrected areas of fragments were used to calculate the transcription ratio. One-way ANOVA and Tukey's multiple-comparison tests were conducted using GraphPad Prism software (GraphPad). All four fragments were sequenced at the University of Wisconsin Biotechnology Center for sequence confirmation.

RESULTS

Retinal phenotypes of $Rs1^{tmgc1}/Rs1^{tmgc1}$ and $Rs1^{tmgc1}$/Y mice improve over time: $Rs1^{tmgc1}/Rs1^{tmgc1}$ and $Rs1^{tmgc1}$/Y mice carry a point mutation in the splice donor site of exon 2 in the *Rs1* gene (Jablonski *et al.* 2005a). These mice are maintained on a mixed background of B6 and C3H. In a previous study, we reported the appearance of the schisis phenotype in these mice by postnatal day (P) 19 (Johnson *et al.* 2006). In this report, we studied the time course of structural changes in the retina of $Rs1^{tmgc1}/Rs1^{tmgc1}$ and $Rs1^{tmgc1}$/Y mice and found that the phenotypes in these mice are the most severe at ~4 weeks of age. Three major morphological phenotypes were observed in $Rs1^{tmgc1}/Rs1^{tmgc1}$ and $Rs1^{tmgc1}$/Y mice at 4 weeks of age: schisis of the inner nuclear layer (INL), waving of the outer nuclear layer (ONL), and ectopic nuclei in the photoreceptor segment layers (Figure 1A). We found that these phenotypes become milder as the mice age. By 10 weeks of age, the schisis phenotype has disappeared but mild layer disorganization is still observed (Figure 1A).

To study the relationship between schisis and retinal function, we also performed ERG analysis at 4 and 9 weeks of age. The ERG a-wave represents the function of the photoreceptor cells while the b-wave is a measure of postsynaptic bipolar cell activity. Mice were studied under dark-adapted conditions to examine the rod pathway. $Rs1^{tmgc1}/Rs1^{tmgc1}$ and $Rs1^{tmgc1}$/Y mice have a reduced b-wave amplitude compared to wild type with a relatively normal a-wave at 4 weeks of age as previously reported (Johnson *et al.* 2006). The a-wave amplitude decreases in $Rs1^{tmgc1}/Rs1^{tmgc1}$ and $Rs1^{tmgc1}$/Y mice from 4 to 9 weeks of age (Figure 1B; ANOVA, $P < 0.0001$). This decrease is likely due to slow photoreceptor cell degeneration or functional loss. In contrast, the amplitude of the b-wave tends to be slightly higher at 9 weeks of age than at 4 weeks of age in $Rs1^{tmgc1}/Rs1^{tmgc1}$ and $Rs1^{tmgc1}$/Y mice, although the difference does not reach statistical significance (Figure 1B). Since the b-wave is measured from the trough of the a-wave to the peak of the b-wave, a decrease in the a-wave amplitude would result in a decrease in the b-wave amplitude. To counteract this effect and to better represent the function of the b-wave generating mechanisms, we calculated the b/a-wave ratio to normalize for the decrease in a-wave that occurs in 9-week-old $Rs1^{tmgc1}/Rs1^{tmgc1}$ and $Rs1^{tmgc1}$/Y mice. At 4 weeks of age, the b/a-wave ratio is significantly decreased in $Rs1^{tmgc1}/Rs1^{tmgc1}$ and $Rs1^{tmgc1}$/Y compared to wild type (ANOVA, $P < 0.0001$; Figure 1C). The b/a-wave ratio in 9-week-old $Rs1^{tmgc1}/Rs1^{tmgc1}$ and $Rs1^{tmgc1}$/Y mice, however, is comparable to that in wild-type mice (Figure 1C). The b/a-wave ratio has significantly improved in 9-week-old mutant mice compared to 4-week-old mutant mice (ANOVA, $P < 0.0001$; Figure 1C). These results suggest that the b-wave generating mechanisms in 9-week-old $Rs1^{tmgc1}/Rs1^{tmgc1}$ and $Rs1^{tmgc1}$/Y mice, including neurotransmission from remaining functional photoreceptor cells to postsynaptic neurons, have improved compared to 4-week-old $Rs1^{tmgc1}/Rs1^{tmgc1}$ and $Rs1^{tmgc1}$/Y mice. This change in retinal function is correlated with the repair of schisis observed over the same period of time.

A major QTL on chromosome 7 rescues the retinal phenotypes in $Rs1^{tmgc1}$/Y mice: In the course of phenotyping F_2 males from an intercross between (AKR × $Rs1^{tmgc1}$/Y) F_1 hybrids, we found that the retinal phenotypes varied among $Rs1^{tmgc1}$/Y F_2 mice at P30 (Figure 2). Large variations were observed only in the F_2 mice that carried the $Rs1^{tmgc1}$ mutation, suggesting the existence of genetic modifiers that specifically interact with the *Rs1* gene. To test the genetic basis of the variation in schisis, we performed a genomewide scan using 45 $Rs1^{tmgc1}$/Y F_2 mice at P30, when the histological phenotypes are the

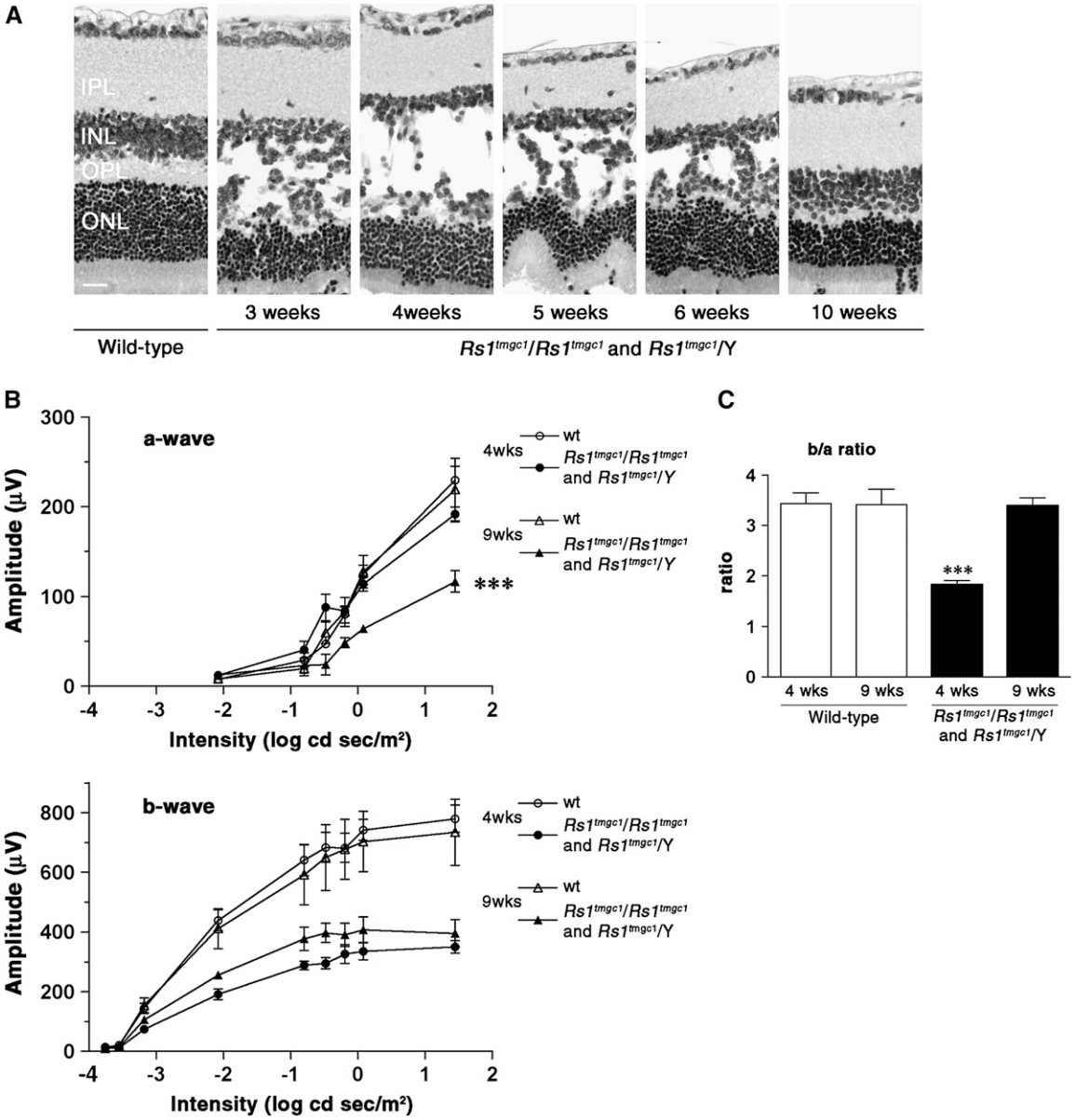

FIGURE 1.—Schisis progression and ERG b-wave response in $Rs1^{tmgc1}/Rs1^{tmgc1}$ and $Rs1^{tmgc1}$/Y mice. (A) Schisis is most severe at 4 weeks of age and decreases over time. Note that adult (10-week-old) $Rs1^{tmgc1}/Rs1^{tmgc1}$ and $Rs1^{tmgc1}$/Y mice do not have schisis. Images of H&E stained paraffin sections are shown. (B) ERG a-wave (top) and b-wave (bottom) responses in $Rs1^{tmgc1}/Rs1^{tmgc1}$ and $Rs1^{tmgc1}$/Y mice at 4 and 9 weeks of age. The graphs show the average response at increasing light intensities for wild-type and $Rs1^{tmgc1}/Rs1^{tmgc1}$ and $Rs1^{tmgc1}$/Y mice. Nine-week-old $Rs1^{tmgc1}/Rs1^{tmgc1}$ and $Rs1^{tmgc1}$/Y mice have a reduced a-wave and slightly higher b-wave amplitude than 4-week-old mice. (C) The b/a-wave ratio in wild-type and $Rs1^{tmgc1}/Rs1^{tmgc1}$ and $Rs1^{tmgc1}$/Y mice at 4 and 9 weeks of age. Nine-week-old $Rs1^{tmgc1}/Rs1^{tmgc1}$ and $Rs1^{tmgc1}$/Y mice have an improved b/a-wave ratio compared to 4-week-old $Rs1^{tmgc1}/Rs1^{tmgc1}$ and $Rs1^{tmgc1}$/Y mice. IPL, inner plexiform layer; INL, inner nuclear layer; OPL, outer plexiform layer; ONL, outer nuclear layer; wt, wild type; bar, 20 μm; $***P < 0.0001$.

most severe in the original 44TNJ strain ($Rs1^{tmgc1}/Rs1^{tmgc1}$ and $Rs1^{tmgc1}$/Y; Figure 1A). Figure 2 shows representative phenotypes in the F_2 population, demonstrating the large phenotypic variation, along with the semiquantitative score (schisis index) given to each. All $Rs1^{tmgc1}$/Y F_2 mice that were phenotyped by histological analysis were also genotyped using microsatellite markers distributed across the entire genome. One major QTL with a large effect was found on Chr 7 (LOD = 6.31, $P < 0.001$) (Figure 3A). Additional markers and animals were used to define the region encompassing the significantly linked QTL on Chr 7. Marker D7Mit321 was most highly associated with the schisis index (LOD = 17.2, $P < 0.0001$, 3 LOD support interval = 46.1–55.1 cM) (Figure 3B). The AKR allele of this QTL significantly reduced the schisis index in $Rs1^{tmgc1}$/Y mice in a recessive fashion (Figure 3C); at least one copy of either the B6 or the C3H allele renders the mice susceptible for the schisis phenotype (Figure 3D). We named the gene responsible for this QTL, the *Mor1* gene.

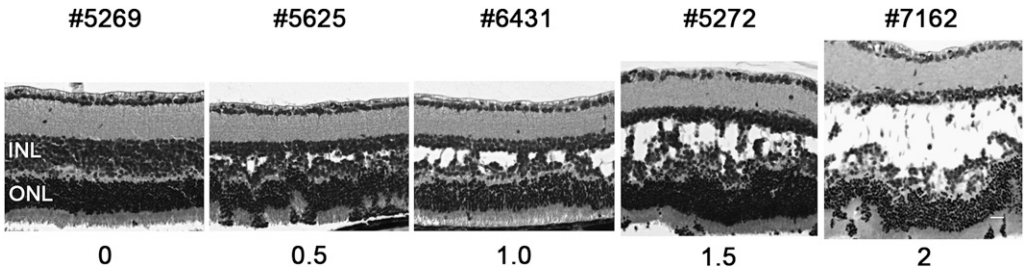

FIGURE 2.—Phenotypic variation in F_2 intercross (AKR × *Rs1*^{tmgc1}/Y) mice. Phenotypic variation observed in *Rs1*^{tmgc1}/Y F_2 mice at P30 with scoring used for the QTL analysis. The numbers at the top of the images are identification numbers of the F_2 mice. The numbers at the bottom represent the semiquantitative scores (schisis index). Images of H&E stained paraffin sections are shown. INL, inner nuclear layer; ONL, outer nuclear layer; bar, 20 μm.

Congenic mice show the allelic effect of *Mor1*: To further test the effect of the *Mor1* gene on the schisis phenotype in *Rs1*^{tmgc1}/Y mice, we generated congenic mice that carry an AKR segment throughout the minimal QTL region of *Mor1* on a B6 genetic background. Male and female congenic mice homozygous for AKR across the QTL region (B6.Cg-*Rs1*^{tmgc1} *Mor1*^{AKR}) were generated by intercrossing N_5 siblings. Among this congenic line, all of the *Mor1*^{AKR}/*Mor1*^{AKR} mice tested ($n = 26$) show normal cell adhesion of the retina at P30 (Figure 4, A and B). In contrast, both *Mor1*^{AKR}/*Mor1*^{B6} and *Mor1*^{B6}/*Mor1*^{B6} mice at P30 show a wide range of phenotypic variation from severe schisis to normal retinal structure (ANOVA, $P < 0.0001$; Figure 4, A and B). This variability is not observed in the original strain of *Rs1*^{tmgc1}/*Rs1*^{tmgc1} and *Rs1*^{tmgc1}/Y (data not shown), which has a mixed genetic background of B6 and C3H (JABLONSKI *et al.* 2005a). Since the *Mor1* congenic region spans the tyrosinase (*Tyr*) locus that is responsible for albinism, all congenic mice that are homozygous for the *Mor1* allele from the albino AKR strain (*Mor1*^{AKR}/*Mor1*^{AKR}) are albino. On the basis of the fact that albinism affects ERG responses (PINTO *et al.* 2007), it was not possible to directly compare the retinal function of *Mor1*^{AKR}/*Mor1*^{AKR} mice to pigmented *Mor1*^{AKR}/*Mor1*^{B6} and *Mor1*^{B6}/*Mor1*^{B6} mice. Our congenic study suggests that (i) one single genetic locus is sufficient to protect *Rs1*^{tmgc1}/*Rs1*^{tmgc1} and *Rs1*^{tmgc1}/Y mice from schisis, (ii) the AKR allele of *Mor1* rescues the phenotype in a recessive fashion, and (iii) the B6 background may have a different effect on phenotypic appearance compared with the mixed genetic background of the original 44TNJ strain.

B6 and C3H congenic lines show a difference in the penetrance of the schisis phenotype: To further understand the origin of the difference in phenotypic variation between B6.Cg-*Rs1*^{tmgc1} mice and the original *Rs1*^{tmgc1}/*Rs1*^{tmgc1} and *Rs1*^{tmgc1}/Y mice (mixed genetic background of B6 and C3H), we generated a second congenic line on a C3H genetic background, C3H.Cg-*Rs1*^{tmgc1} and tested the appearance of the schisis phenotype at P30. We observed that 92% ($n = 12/13$) of C3H.Cg-*Rs1*^{tmgc1} mice (N_5–N_9 generations) show the schisis phenotype (Figure 5). This is in contrast to the phenotypic distribution of B6.Cg-*Rs1*^{tmgc1} mice (N_5–N_9 generations) shown in Figure 5, in which only 37% ($n = 14/38$ total) of the B6.Cg-*Rs1*^{tmgc1} mice have schisis (χ^2, $P < 0.0006$). Our results show that the difference in the genetic background affects the penetrance of the schisis phenotype in *Rs1* mutant mice.

Quantifying the ratio of differentially spliced transcripts from *Rs1*: *Rs1*^{tmgc1}/*Rs1*^{tmgc1} and *Rs1*^{tmgc1}/Y mice have a point mutation in the splice donor site of exon 2 (JABLONSKI *et al.* 2005a). Previously, we reported that the mutation causes aberrant splice products in *Rs1*^{tmgc1}/*Rs1*^{tmgc1} and *Rs1*^{tmgc1}/Y mice (JOHNSON *et al.* 2006). To examine whether the age of *Rs1*^{tmgc1}/*Rs1*^{tmgc1} and *Rs1*^{tmgc1}/Y mice or the genotype of *Mor1* affects the splice population, we performed fragment analysis of *Rs1* transcripts. Fragment analysis of RT–PCR products from B6 mice identified a single 738-bp transcript (Figure 6A). On the basis of our previous study to sequence subclones of RT–PCR products, the B6 retina appears to have a single wild-type transcript (JOHNSON *et al.* 2006). In contrast, at least three alternative transcripts in mice carry a mutation in the *Rs1* gene including *Rs1*^{tmgc1}/*Rs1*^{tmgc1} and *Rs1*^{tmgc1}/Y mice (Figure 6A) and *Mor1*^{AKR}/*Mor1*^{AKR} and *Mor1*^{B6}/*Mor1*^{B6} congenic mice. These alternative transcripts result from the deletion of exon 2, deletion of exons 2 and 3, or an intronic retention to the wild-type transcript following exon 2 (JOHNSON *et al.* 2006) (Figure 6B). In all three mutant lines including *Rs1*^{tmgc1}/*Rs1*^{tmgc1} and *Rs1*^{tmgc1}/Y mice at 4 weeks of age and *Rs1*^{tmgc1}/*Rs1*^{tmgc1} mice at 16 weeks of age, the percentage of wild-type transcripts was ~30% of the total, transcripts with exon 2 deleted were ~41%, and transcripts with exons 2 and 3 deleted were ~22% (Figure 6C). Transcripts with intronic retention were ~7% in all mutant lines at 4 weeks of age (Figure 6C). The ratio of each transcript class to the total was not statistically different among the different genetic backgrounds or among different developmental stages (4-week-old *Rs1*^{tmgc1}/*Rs1*^{tmgc1} and *Rs1*^{tmgc1}/Y mice *vs.* 16-week-old *Rs1*^{tmgc1}/*Rs1*^{tmgc1}) with the exception of the wild-type + intronic transcript, where 16-week-old *Rs1*^{tmgc1}/*Rs1*^{tmgc1} mice had a significantly higher ratio (10.6%) compared to *Mor1*^{B6}/*Mor1*^{B6} congenic mice (5%; ANOVA, $P < 0.05$).

DISCUSSION

In this study, we show that genetic factors are important to determine the severity and penetrance of XLRS phenotypes observed in *Rs1* mutant mice.

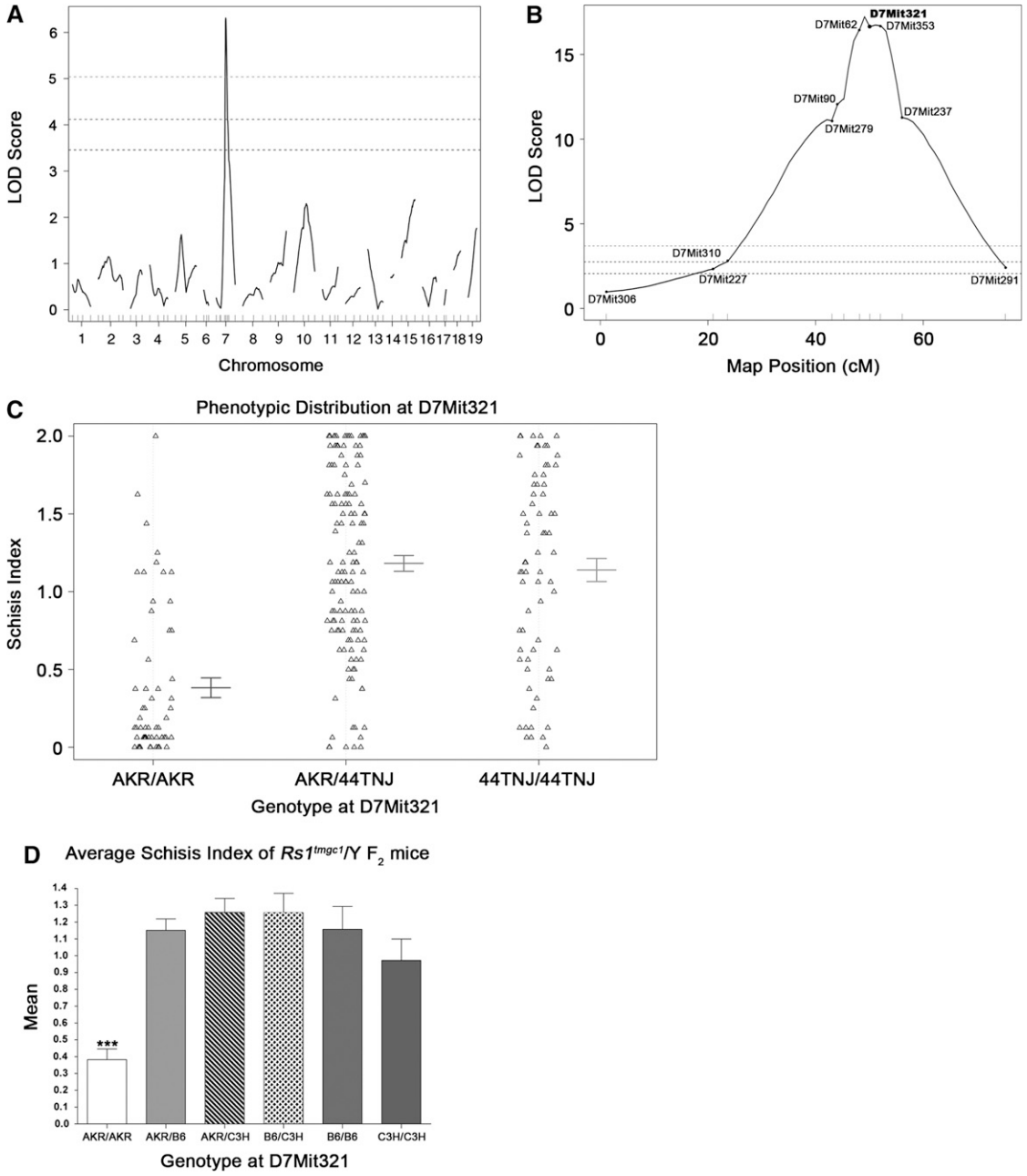

FIGURE 3.—QTL mapping of the modifier of *Rs1*. (A) Whole genome scan LOD score distribution for association of the schisis index in 45 $Rs1^{tmgc1}$/Y F_2 intercross mice. The QTL on Chr 7 was named *Mor1* for **m**odifier **o**f ***Rs1*** **1**. Three horizontal lines represent significant linkage as assessed by permutation testing (bottom, $P < 0.05$; middle, $P < 0.01$; top, $P < 0.001$). (B) LOD score distribution on Chr 7 for all $Rs1^{tmgc1}$/Y F_2 mice. After *Mor1* was identified in the whole genome scan, 225 additional mice were genotyped and phenotyped for Chr 7. The LOD score distribution for the total 270 $Rs1^{tmgc1}$/Y F_2 intercross mice is shown. The genetic map was generated in R/qtl on the basis of our cross. D7Mit321 is the marker that is closest to the peak LOD score of 17.2 ($P < 0.0001$). Three horizontal lines represent significant linkage as noted in A. (C) Phenotypic distribution of F_2 mice at D7Mit321. Error bars represent ±1 standard error. 44TNJ includes both B6 and C3H alleles. (D) Mean schisis index of $Rs1^{tmgc1}$/Y F_2 mice with respect to AKR, B6, and C3H alleles. B6 and C3H alleles render the severe phenotype. Only mice that are AKR/AKR at D7Mit321 show significant reduction of the schisis index (ANOVA, $P < 0.0001$).

$Rs1^{tmgc1}$/Y F_2 mice showed a wide range of phenotypic severity, indicating the existence of genetic factors that affect these phenotypes. We identified a major QTL named *Mor1*, which is a single locus that acts as a recessive suppressor for the schisis phenotype. The protective (AKR) allele of *Mor1,* when homozygous, restored cell adhesion in B6.Cg-$Rs1^{tmgc1}$ $Mor1^{AKR}$ mice. Our results also suggest that an allelic difference in the genetic background between B6 and C3H affects the penetrance of the retinoschisis phenotype.

***Mor1* is a major QTL:** It has been hypothesized that RS1 is involved in cell adhesion on the basis of its

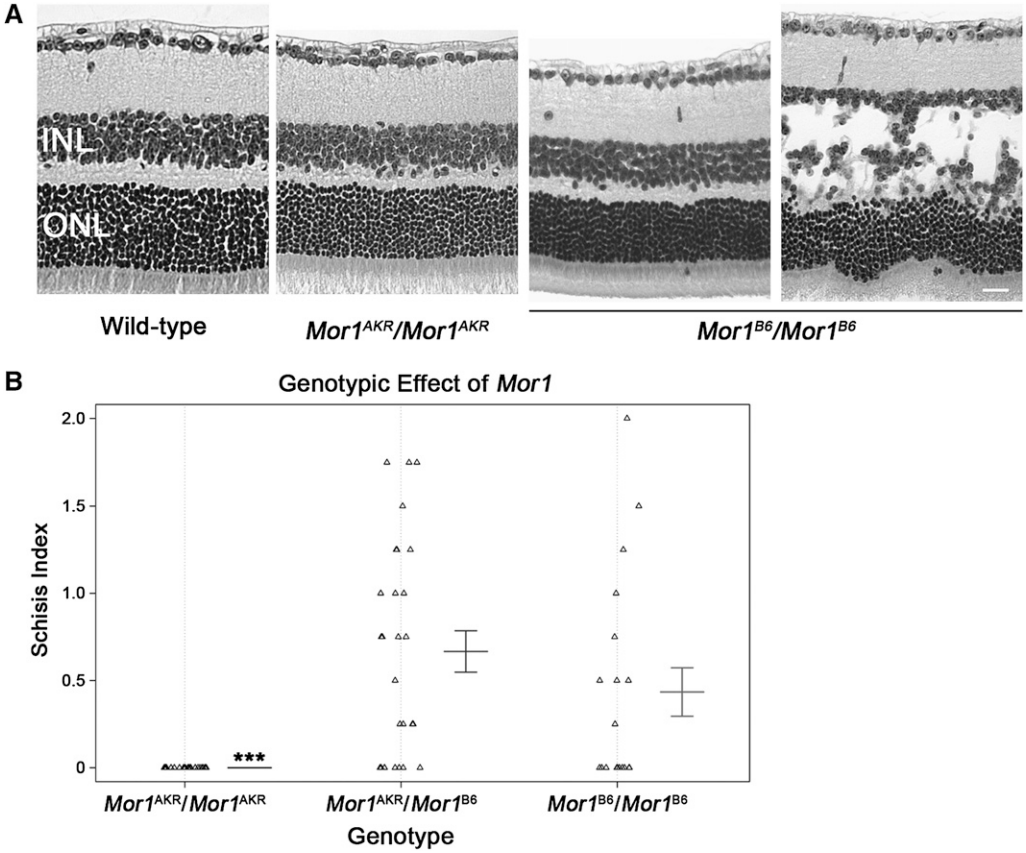

FIGURE 4.—*Mor1* allelic differences in B6 congenic mice. (A) Images are representative of the phenotypes in the B6 congenic (B6.Cg-*Rs1*^{tmgc1}) line at P30. All *Mor1*^{AKR}/*Mor1*^{AKR} mice do not exhibit the schisis phenotype. *Mor1*^{AKR}/*Mor1*^{B6} (images not shown) and *Mor1*^{B6}/*Mor1*^{B6} mice have a range of phenotypic severity from no schisis to severe schisis. Images of H&E stained paraffin sections are shown. (B) The scatter plot shows the genotypic effect of *Mor1* on phenotypic severity in congenic mice. INL, inner nuclear layer; ONL, outer nuclear layer; bar, 20 μm; ***, ANOVA $P < 0.0001$.

localization at the cell surface and schisis-like phenotypes in both human XLRS patients and in mouse models carrying *Rs1* gene mutations (SAUER *et al.* 1997; RETINOSCHISIS CONSORTIUM 1998; WEBER *et al.* 2002; ZENG *et al.* 2004; WU *et al.* 2005; MOLDAY *et al.* 2007; VIJAYASARATHY *et al.* 2007). Our results show that a single locus, *Mor1*, can specifically modify cell adhesion and other retinal phenotypes in *Rs1*^{tmgc1}/*Rs1*^{tmgc1} and *Rs1*^{tmgc1}/Y mice. The effect of the allelic difference of the *Mor1* gene on maintenance of cell adhesion is not observed in wild-type mice, however, the allelic effect becomes significant when RS1 does not function properly. This finding suggests an epistatic interaction between *Rs1* and *Mor1*.

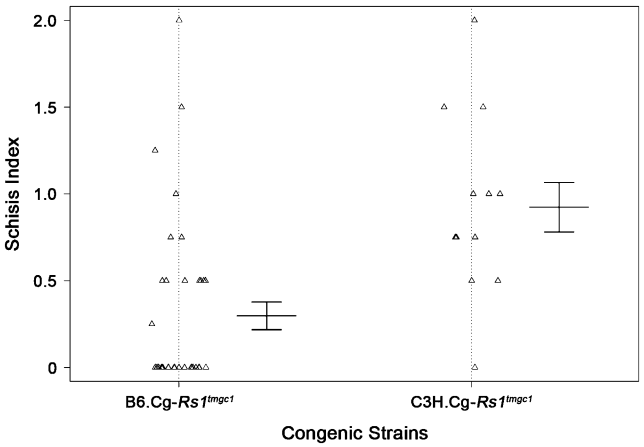

FIGURE 5.—Penetrance of the schisis phenotype in B6 and C3H congenic mice. Phenotypic distribution of B6 (B6.Cg-*Rs1*^{tmgc1}) and C3H (C3H.Cg-*Rs1*^{tmgc1}) congenic mice at P30. The penetrance of the schisis phenotype is significantly different between the two congenic strains (χ^2, $P < 0.0006$). Thirty-seven percent of the B6 congenic mice have the schisis phenotype, whereas 92% of the C3H congenic mice have schisis.

Possible roles of MOR1: The protective allele of *Mor1* may restore cell adhesion in *Rs1*^{tmgc1}/*Rs1*^{tmgc1} and *Rs1*^{tmgc1}/Y mice in several ways. One possibility is that MOR1 may be directly involved in the molecular pathway in which RS1 functions as a mediator of cell adhesion. In *Rs1*^{tmgc1}/*Rs1*^{tmgc1} and *Rs1*^{tmgc1}/Y retinas, 30% of *Rs1* transcripts are normally spliced. MOR1 may be able to specifically interact with the normal RS1 and enhance its function in the diseased retina or MOR1 may be able to directly replace RS1 when RS1 is nonfunctional. MOR1 could also function in a parallel pathway involved in cell adhesion that, when in the presence of a mutant RS1, is upregulated and can compensate for the loss of RS1-mediated cell adhesion.

Alternatively, we hypothesize that MOR1 may affect the population of transcripts in *Rs1*^{tmgc1}/*Rs1*^{tmgc1} and *Rs1*^{tmgc1}/Y retinas. *Rs1*^{tmgc1}/*Rs1*^{tmgc1} and *Rs1*^{tmgc1}/Y mice harbor a T-to-C point mutation in the splice donor site of exon 2 (JABLONSKI *et al.* 2005a). The mutation causes

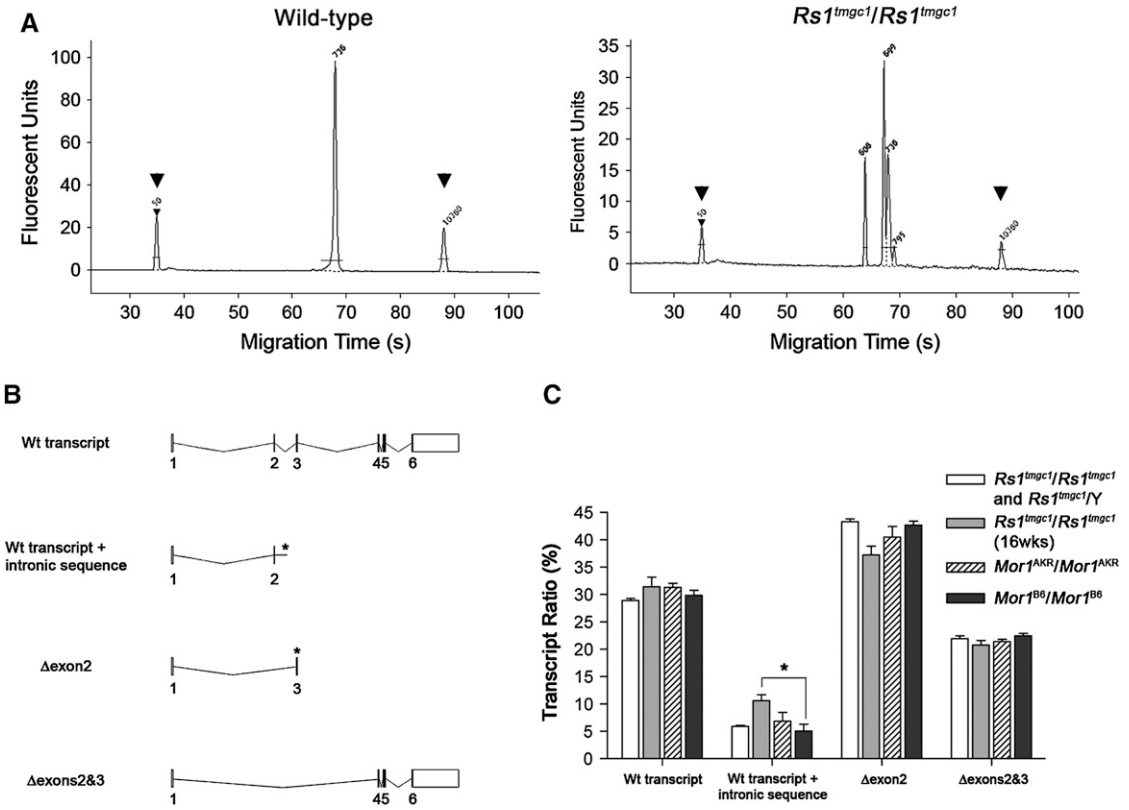

FIGURE 6.—Population of transcripts in *Rs1*^{tmgc1}/*Rs1*^{tmgc1} and *Rs1*^{tmgc1}/Y and B6 congenic mice. (A) Representative electropherograms for *Rs1* transcripts in the mouse retina. Wild-type mice show one major peak corresponding to the full-length wild-type transcript (738 bp), while male and female *Rs1*^{tmgc1} mutant mice show a full-length transcript plus three alternative transcripts at 609 bp, 699 bp, and 787 bp. Control peaks are labeled with arrowheads. (B) Splicing variants of *Rs1*. The diagram illustrates the mouse *Rs1* wild-type transcript and the three splice variants found in *Rs1*^{tmgc1}/*Rs1*^{tmgc1} and *Rs1*^{tmgc1}/Y retinas. The asterisks denote the formation of premature stop codons. (C) Relative amount of transcript variants found in *Rs1*^{tmgc1}/*Rs1*^{tmgc1} and *Rs1*^{tmgc1}/Y retinas. The amount of each transcript variant is shown as a percentage of total transcripts in *Rs1*^{tmgc1}/*Rs1*^{tmgc1} and *Rs1*^{tmgc1}/Y mice and B6 congenic (B6.Cg-*Rs1*^{tmgc1}) mice that are *Mor1*^{AKR}/*Mor1*^{AKR} or *Mor1*^{B6}/*Mor1*^{B6}. Mice were tested at 4 weeks of age unless noted. The ratios for wild-type transcripts, transcripts that skip exon 2, and transcripts that skip both exons 2 and 3 are not significantly different among all groups tested. The ratio of wild-type transcripts with intronic sequence is significantly different ($P < 0.05$) between *Mor1*^{B6}/*Mor1*^{B6} and 16-week-old *Rs1*^{tmgc1}/*Rs1*^{tmgc1} mice.

aberrant splicing which leads to transcripts with skipped exons or cryptic splice sites (JOHNSON *et al.* 2006). Nevertheless, ~30% of the *Rs1* transcripts are spliced normally. We hypothesized that MOR1 could be a part of the splice machinery, in which case the AKR variant of MOR1 could increase the proportion of correctly spliced *Rs1* products. Recently in another mouse model of disease, it was reported that a splice-site variant modifies disease severity (HOWELL *et al.* 2007). The B6 variant of the sodium channel modifier 1 (SCNM1), an RNA splicing factor, has been shown to modify disease severity in *Scn8a*$^{med/J}$ mice (BUCHNER *et al.* 2003; HOWELL *et al.* 2007). After performing the fragment analysis (Figure 6), however, it is unlikely that *Mor1* is involved in RNA splicing.

The effect of *Mor1* on retinal function: To test whether the function of the retinal neurons is also restored in *Mor1*^{AKR}/*Mor1*^{AKR} congenic mice, ERG analysis comparing congenic mice with different genotypes at the *Mor1* locus would be ideal. However, a difference between these strains exists that interferes with this comparison. All mice that are homozygous for AKR across the *Mor1* candidate region (*Mor1*^{AKR}/*Mor1*^{AKR}) are homozygous for a recessive mutation in the tyrosinase gene (*Tyr*^{c}). The *Tyr* locus resides between markers D7Mit62 and D7Mit321, which are near the peak LOD score in the *Mor1* candidate region. Homozygosity for the recessive *Tyr*^{c} allele renders these mice albino with nonpigmented eyes, while mice that are *Mor1*^{B6}/*Mor1*^{AKR}, *Mor1*^{B6}/*Mor1*^{B6}, and *Mor1*^{C3H}/*Mor1*^{C3H} are pigmented and have pigmented eyes. Since albinism affects ERGs by increasing retinal illumination through light reflected from the back of the eye (PINTO *et al.* 2007), a direct comparison between the ERG waves of congenic mice that are *Mor1*^{AKR}/*Mor1*^{AKR} with the ERGs of mice that have pigmented eyes is not appropriate. Further identification of the *Mor1* gene will allow us to directly test the role of the *Mor1* gene on retinal function using genetically engineered mice or congenic mice that have a crossover between the *Tyr* locus and the *Mor1* gene.

Natural rescue: In *Rs1*^{tmgc1}/*Rs1*^{tmgc1} and *Rs1*^{tmgc1}/Y mice (the original strain of mice that are not homozygous for the protective allele of *Mor1*), we consistently observe restoration of cell adhesion by 10 weeks of age (Figure 1). A compensatory pathway involved in cell adhesion may turn on naturally in aged *Rs1*^{tmgc1}/*Rs1*^{tmgc1} and *Rs1*^{tmgc1}/Y mice that rescues the schisis phenotype. It is possible that MOR1 may be involved in both restoration of cell adhesion at an early age (P30) and natural rescue at an older age. For example, the AKR allele of *Mor1* could contain a polymorphism in the *Mor1* promoter region, which causes *Mor1* expression to be turned on at a younger age. This natural schisis rescue has also been reported in a knockout model of *Rs1* (Kjellstrom *et al.* 2007). The time course of rescue is different in knockout mice, which show the most severe phenotypes at 4 months of age (Kjellstrom *et al.* 2007) whereas phenotypes in *Rs1*^{tmgc1}/*Rs1*^{tmgc1} and *Rs1*^{tmgc1}/Y mice are most severe at 4 weeks of age. Nevertheless, the same molecular mechanism for rescuing schisis may be shared by the two mouse strains. In human XLRS patients, natural improvement of disease phenotypes over time (such as spontaneous reattachment and increased visual acuity) have also been reported (George *et al.* 1995a,b, 1996; Apushkin *et al.* 2005).

Candidate genes: Genes that are expressed in the retina and known to be involved in cell adhesion could be candidates for *Mor1*. Although the minimal genetic region of *Mor1* is still large (9 cM on the basis of our genetic map, which is encompassed in the region between D7Mit279 and D7Mit237, ~635 annotated genes), preliminary examination of the *Mor1* region identifies some interesting candidate genes. Genes that encode transmembrane, membrane-associated, extracellular matrix proteins, or proteins involved in synaptic stability are attractive candidates for *Mor1*. For example, discs large homolog 2 (*Dlg2*), located between markers D7Mit62 and D7Mit321, encodes a scaffolding protein involved in stabilization of cholinergic synapses (Parker *et al.* 2004). Other genes within the *Mor1* region that encode transmembrane proteins, membrane-associated proteins, or extracellular matrix proteins include transmembrane proteins 126, a and b (*Tmem126a* and *Tmem126b*), transmembrane protein 135 (*Tmem135*), odd Oz/ten-m homolog 4 (*Odz4*), tsukushin (*Tsku*), and frizzled homolog 4 (Fdz4).

Genetic variability is the cause for differences in the penetrance of the schisis phenotype in *Rs1*^{tmgc}/*Rs1*^{tmgc1} and *Rs1*^{tmgc1}/Y mice: We found that C3H.Cg-*Rs1*^{tmgc1} mice have a higher penetrance of the schisis phenotype than B6.Cg-*Rs1*^{tmgc1} mice (Figure 5). From these results we hypothesize that there may be another modifier(s) that affects the penetrance of the schisis phenotype. Since F_2 mice with either B6 or C3H across Chr 7 have the severe phenotype (Figure 3D), this second modifier is most likely not on Chr 7. The original *Rs1*^{tmgc1} (44TNJ) line may always have the severe phenotype because the majority of the genetic background in these mice is C3H. Similar genetic background effects on the penetrance of phenotypes have been previously reported (reviewed in Nadeau 2001). For example, the penetrance of the multiple birth defects caused by the disorganization (*Ds*) mutation ranges from 89% penetrance on a C3H background to as low as 0% on a B6 background (Hummel 1958). It has been hypothesized that environmental factors such as diet and light may affect the phenotypic variability observed in *Rs1* knockout mice (Kjellstrom *et al.* 2007). The results of our study suggest that genetic factors also have a major effect in the appearance of the retinoschisis phenotype. It is possible that these genetic factors may interact with some environmental factors, thereby changing the susceptibility to the environment.

Relevance to human XLRS: In human XLRS patients, there is large variability in the severity of phenotypes caused by a particular *RS1* mutation. Numerous cases have been documented where family members with the exact same *RS1* mutation have a wide range of phenotypic severity, which suggests the existence of genetic modifiers (Eksandh *et al.* 2000; Pimenides *et al.* 2005). Searching for modifiers in humans is challenging due to heterogeneous genetic backgrounds. The mouse provides a powerful tool to search for and identify modifier genes. Following the identification of modifier genes in mice, the same modifiers can be examined in human patients. *Mor1* is the first modifier of *Rs1* identified to date. Identification of the causative gene of *Mor1* will not only provide insight into the function of RS1, but may also provide insight into the genotype–phenotype disparity observed in human XLRS patients and elucidate novel therapeutic approaches for XLRS.

The authors thank Angela Verdoni and Xinjie Xu for critical review of this manuscript. The authors also thank the Tennessee Mouse Genome Consortium (TMGC) ENU mutagenesis project for generating and providing 44TNJ mice. This project was supported by grants to A.I. from the National Institutes of Health (R01 EY016394), The Rebecca Meyer Brown pilot project award professorship from the Retina Research Foundation, and an Individual Investigator grant from the Foundation Fighting Blindness. B.J. was partially supported by the National Institutes of Health Predoctoral Training Program in Genetics from the University of Wisconsin, Madison (5 T32 GM07133).

LITERATURE CITED

Apushkin, M. A., G. A. Fishman and A. S. Rajagopalan, 2005 Fundus findings and longitudinal study of visual acuity loss in patients with X-linked retinoschisis. Retina **25:** 612–618.

Baumgartner, S., K. Hofmann, R. Chiquet-Ehrismann and P. Bucher, 1998 The discoidin domain family revisited: new members from prokaryotes and a homology-based fold prediction. Protein Sci. **7:** 1626–1631.

Blackburn, A. C., L. Z. Hill, A. L. Roberts, J. Wang, D. Aud *et al.*, 2007 Genetic mapping in mice identifies DMBT1 as a candidate modifier of mammary tumors and breast cancer risk. Am. J. Pathol. **170:** 2030–2041.

Broman, K. W., H. Wu, S. Sen and G. A. Churchill, 2003 R/qtl: QTL mapping in experimental crosses. Bioinformatics **19:** 889–890.

Buchner, D. A., M. Trudeau and M. H. Meisler, 2003 SCNM1, a putative RNA splicing factor that modifies disease severity in mice. Science **301:** 967–969.

Clee, S. M., B. S. Yandell, K. M. Schueler, M. E. Rabaglia, O. C. Richards *et al.*, 2006 Positional cloning of Sorcs1, a type 2 diabetes quantitative trait locus. Nat. Genet. **38:** 688–693.

Eksandh, L. C., V. Ponjavic, R. Ayyagari, E. L. Bingham, K. T. Hiriyanna *et al.*, 2000 Phenotypic expression of juvenile X-linked retinoschisis in Swedish families with different mutations in the XLRS1 gene. Arch. Ophthalmol. **118:** 1098–1104.

George, N. D., J. R. Yates, K. Bradshaw and A. T. Moore, 1995a Infantile presentation of X linked retinoschisis. Br. J. Ophthalmol. **79:** 653–657.

George, N. D., J. R. Yates and A. T. Moore, 1995b X linked retinoschisis. Br. J. Ophthalmol. **79:** 697–702.

George, N. D., J. R. Yates and A. T. Moore, 1996 Clinical features in affected males with X-linked retinoschisis. Arch. Ophthalmol. **114:** 274–280.

Goodarzi, M. O., D. M. Lehman, K. D. Taylor, X. Guo, J. Cui *et al.*, 2007 SORCS1: a novel human type 2 diabetes susceptibility gene suggested by the mouse. Diabetes **56:** 1922–1929.

Harris, G. S., and J. Yeung, 1976 Maculopathy of sex-linked juvenile retinoschisis. Can. J. Ophthalmol. **11:** 1–10.

Hewitt, A. W., L. M. FitzGerald, L. W. Scotter, L. E. Mulhall, J. D. McKay *et al.*, 2005 Genotypic and phenotypic spectrum of X-linked retinoschisis in Australia. Clin. Exp. Ophthalmol. **33:** 233–239.

Hiraoka, M., M. T. Trese and B. S. Shastry, 2000 X–Linked juvenile retinoschisis associated with a 4-base pair insertion at codon 55 of the XLRS1 gene. Biochem. Biophys. Res. Commun. **268:** 370–372.

Howell, V. M., J. M. Jones, S. Bergren, L. Li, A. C. Billi *et al.*, 2007 Evidence for a direct role of the disease modifier SCNM1 in splicing. Hum. Mol. Genet. **16:** 3506–3516.

Hummel, K. P., 1958 The inheritance and expression of disorganization, an unusual mutation in the mouse. J. Exp. Zool. **137:** 389–423.

Jablonski, M. M., C. Dalke, X. Wang, L. Lu, K. F. Manly *et al.*, 2005a An ENU-induced mutation in Rs1h causes disruption of retinal structure and function. Mol. Vis. **11:** 569–581.

Jablonski, M. M., X. Wang, L. Lu, D. R. Miller, E. M. Rinchik *et al.*, 2005b The Tennessee Mouse Genome Consortium: identification of ocular mutants. Vis. Neurosci. **22:** 595–604.

Johnson, B. A., S. Ikeda, L. H. Pinto and A. Ikeda, 2006 Reduced synaptic vesicle density and aberrant synaptic localization caused by a splice site mutation in the Rs1h gene. Vis. Neurosci. **23:** 887–898.

Kellner, U., S. Brummer, M. H. Foerster and A. Wessing, 1990 X-linked congenital retinoschisis. Graefes Arch. Clin. Exp. Ophthalmol. **228:** 432–437.

Kjellstrom, S., R. A. Bush, Y. Zeng, Y. Takada and P. A. Sieving, 2007 Retinoschisin gene therapy and natural history in the Rs1h-KO mouse: long-term rescue from retinal degeneration. Invest. Ophthalmol. Vis. Sci. **48:** 3837–3845.

Min, S. H., L. L. Molday, M. W. Seeliger, A. Dinculescu, A. M. Timmers *et al.*, 2005 Prolonged recovery of retinal structure/function after gene therapy in an Rs1h-deficient mouse model of x-linked juvenile retinoschisis. Mol. Ther. **12:** 644–651.

Molday, L. L., D. Hicks, C. G. Sauer, B. H. Weber and R. S. Molday, 2001 Expression of X-linked retinoschisis protein RS1 in photoreceptor and bipolar cells. Invest. Ophthalmol. Vis. Sci. **42:** 816–825.

Molday, L. L., W. W. Wu and R. S. Molday, 2007 Retinoschisin (RS1), the protein encoded by the X-linked retinoschisis gene, is anchored to the surface of retinal photoreceptor and bipolar cells through its interactions with a Na/K ATPase-SARM1 complex. J. Biol. Chem. **282:** 32792–32801.

Nadeau, J. H., 2001 Modifier genes in mice and humans. Nat. Rev. Genet. **2:** 165–174.

Nadeau, J. H., 2003 Modifier genes and protective alleles in humans and mice. Curr. Opin. Genet. Dev. **13:** 290–295.

Nakamura, M., S. Ito, H. Terasaki and Y. Miyake, 2001 Japanese X-linked juvenile retinoschisis: conflict of phenotype and genotype with novel mutations in the XLRS1 gene. Arch. Ophthalmol. **119:** 1553–1554.

Parker, M. J., S. Zhao, D. S. Bredt, J. R. Sanes and G. Feng, 2004 PSD93 regulates synaptic stability at neuronal cholinergic synapses. J. Neurosci. **24:** 378–388.

Peachey, N. S., G. A. Fishman, D. J. Derlacki and M. G. Brigell, 1987 Psychophysical and electroretinographic findings in X-linked juvenile retinoschisis. Arch. Ophthalmol. **105:** 513–516.

Pimenides, D., N. D. George, J. R. Yates, K. Bradshaw, S. A. Roberts *et al.*, 2005 X-linked retinoschisis: clinical phenotype and RS1 genotype in 86 UK patients. J. Med. Genet. **42:** e35.

Pinto, L. H., M. H. Vitaterna, S. M. Siepka, K. Shimomura, S. Lumayag *et al.*, 2004 Results from screening over 9000 mutation-bearing mice for defects in the electroretinogram and appearance of the fundus. Vision Res. **44:** 3335–3345.

Pinto, L. H., B. Invergo, K. Shimomura, J. S. Takahashi and J. B. Troy, 2007 Interpretation of the mouse electroretinogram. Doc. Ophthalmol. **115:** 127–136.

Reid, S. N., N. B. Akhmedov, N. I. Piriev, C. A. Kozak, M. Danciger *et al.*, 1999 The mouse X-linked juvenile retinoschisis cDNA: expression in photoreceptors. Gene **227:** 257–266.

Retinoschisis Consortium, 1998 Functional implications of the spectrum of mutations found in 234 cases with X-linked juvenile retinoschisis. Hum. Mol. Genet. **7:** 1185–1192.

Roesch, M. T., C. C. Ewing, A. E. Gibson and B. H. Weber, 1998 The natural history of X-linked retinoschisis. Can. J. Ophthalmol. **33:** 149–158.

Sauer, C. G., A. Gehrig, R. Warneke-Wittstock, A. Marquardt, C. C. Ewing *et al.*, 1997 Positional cloning of the gene associated with X-linked juvenile retinoschisis. Nat. Genet. **17:** 164–170.

Seiving, P., 1998 Juvenile retinoschisis, pp. 347–356 in *Genetic Diseases of the Eye*, edited by E. Traboulsi. Oxford University Press, New York.

Sen, S., and G. A. Churchill, 2001 A statistical framework for quantitative trait mapping. Genetics **159:** 371–387.

Shinoda, K., Y. Mashima, S. Ishida and Y. Oguchi, 1999 Severe juvenile retinoschisis associated with a 33-bps deletion in XLRS1 gene. Ophthalmic Genet. **20:** 57–61.

Simonelli, F., G. Cennamo, C. Ziviello, F. Testa, G. de Crecchio *et al.*, 2003 Clinical features of X linked juvenile retinoschisis associated with new mutations in the XLRS1 gene in Italian families. Br. J. Ophthalmol. **87:** 1130–1134.

Takada, Y., R. N. Fariss, M. Muller, R. A. Bush, E. J. Rushing *et al.*, 2006 Retinoschisin expression and localization in rodent and human pineal and consequences of mouse RS1 gene knockout. Mol. Vis. **12:** 1108–1116.

Takada, Y., R. N. Fariss, A. Tanikawa, Y. Zeng, D. Carper *et al.*, 2004 A retinal neuronal developmental wave of retinoschisin expression begins in ganglion cells during layer formation. Invest. Ophthalmol. Vis. Sci. **45:** 3302–3312.

Vijayasarathy, C., Y. Takada, Y. Zeng, R. A. Bush and P. A. Sieving, 2007 Retinoschisin is a peripheral membrane protein with affinity for anionic phospholipids and affected by divalent cations. Invest. Ophthalmol. Vis. Sci. **48:** 991–1000.

Weber, B. H., H. Schrewe, L. L. Molday, A. Gehrig, K. L. White *et al.*, 2002 Inactivation of the murine X-linked juvenile retinoschisis gene, Rs1h, suggests a role of retinoschisin in retinal cell layer organization and synaptic structure. Proc. Natl. Acad. Sci. USA **99:** 6222–6227.

Wu, W. W., and R. S. Molday, 2003 Defective discoidin domain structure, subunit assembly, and endoplasmic reticulum processing of retinoschisin are primary mechanisms responsible for X-linked retinoschisis. J. Biol. Chem. **278:** 28139–28146.

Wu, W. W., J. P. Wong, J. Kast and R. S. Molday, 2005 RS1, a discoidin domain-containing retinal cell adhesion protein associated with X-linked retinoschisis, exists as a novel disulfide-linked octamer. J. Biol. Chem. **280:** 10721–10730.

Zeng, Y., Y. Takada, S. Kjellstrom, K. Hiriyanna, A. Tanikawa *et al.*, 2004 RS-1 gene delivery to an adult Rs1h knockout mouse model restores ERG b-wave with reversal of the electronegative waveform of X-linked retinoschisis. Invest. Ophthalmol. Vis. Sci. **45:** 3279–3285.

Communicating editor: T. R. Magnuson